JOURNAL OF AIRCRAFT
Vol. 45, No. 2, March–April 2008

Aerodynamic Simulation of a Horn-Ice Accretion on a Subscale Model

Greg T. Busch,* Andy P. Broeren,† and Michael B. Bragg‡
University of Illinois at Urbana–Champaign, Urbana, Illinois 61801

DOI: 10.2514/1.32338

The objective of this experimental investigation was to determine the geometric simulation fidelity required to accurately model the aerodynamics of a horn-ice accretion in a wind tunnel. A casting and a 2-D smooth simulation with variable horn geometry were constructed to model a horn-ice accretion on a NACA 0012 airfoil. Several simulations of differing fidelity, including a casting, were constructed to model a horn-ice accretion on a NACA 23012 airfoil. Aerodynamic testing was performed in the University of Illinois 3 × 4 ft wind tunnel at a Reynolds number of 1.8×10^6 and a Mach number of 0.18. Minor changes to the upper-horn geometry of the NACA 0012 2-D smooth simulation were found to have notable impacts on drag and maximum lift. Therefore, spanwise variations in the ice accretion geometry must be carefully examined so that an appropriate cross section can be chosen from which to generate a tracing for a 2-D simulation. Such a 2-D smooth simulation, as was constructed for the NACA 23012 airfoil, can model maximum lift to within 1% of that of the casting. This type of simulation can also provide an estimate of drag that is within the uncertainty of the casting due to spanwise variation, although it does not reproduce three dimensionality in the iced-airfoil flowfield.

Nomenclature

C_d	=	drag coefficient
$C_{d,\min}$	=	minimum drag coefficient
C_l	=	lift coefficient
$C_{l,\max}$	=	maximum lift coefficient
C_m	=	quarter-chord pitching-moment coefficient
C_p	=	pressure coefficient
c	=	airfoil chord length
k	=	feature height
M	=	freestream Mach number
Re	=	freestream Reynolds number, based on the airfoil chord length
s	=	airfoil model coordinate along the surface length
x	=	coordinate in the airfoil model chordwise direction
α	=	airfoil angle of attack
θ	=	ice-shape horn angle with respect to the chord line

Introduction

TO PROMOTE safety and reliability of operations, aircraft are certified for flight into icing conditions. Manufacturers can achieve this certification in part by demonstrating that their aircraft can fly safely after an ice accretion has formed. This is difficult to do in flight tests using a natural ice accretion, as it is hard to find a large uniform icing cloud with the desired conditions. Therefore, simulations are often used to represent the ice accretion aerodynamically in a wind tunnel. These simulations can have a very high fidelity, capturing all of the three dimensionality and roughness of the actual ice accretion, or they can be of lower fidelity, representing only the main features of the ice accretion using simple geometric (SG) shapes such as triangles or rectangles. High-fidelity simulations are expensive and time consuming to produce, so it is often necessary to use lower-fidelity simulations. This paper investigates the use of simulations of varying fidelity to determine the aerodynamics of a horn-ice accretion and makes recommendations as to the fidelity required to accurately assess horn-ice accretion effects. This work was conducted as part of a research program described by Bragg et al. [1] which considers three other types of ice accretions in addition to the horn ice presented here.

Horn-ice accretions typically form at temperatures just below freezing when water droplets impinge on the airfoil, form a wet surface, and later freeze. These droplets eventually coalesce into a protrusion referred to as a horn. A horn may form on only the upper surface or on both the upper and lower surfaces, depending on the icing conditions. The horn itself has a rough and irregular surface. Behind it is often a region of highly three-dimensional ice feathers and nodules.

Bragg et al. [2] have identified the key aerodynamic characteristics of a horn-ice accretion. The sharp tip of the horn introduces a severe adverse pressure gradient, causing the boundary layer to separate. The shear layer between the separated flow behind the horn and the inviscid flow over the top of the horn eventually becomes turbulent, reenergizing the low-momentum separated flow and promoting reattachment. As the airfoil angle of attack increases, the reattachment location moves farther downstream on the airfoil surface. At some angle of attack, it moves off the surface of the airfoil, and the airfoil becomes completely stalled. The separation bubble, similar to the long bubble described by Tani [3], dominates the airfoil aerodynamics, with larger bubbles causing greater penalties to lift and drag. The size of the separation bubble on a given airfoil at a given angle of attack is determined by the main geometric characteristics of the horn, such as horn height (k/c), horn location (s/c), horn angle (θ), and sometimes horn tip radius (r/c). Horn-ice accretions generally cause a severe reduction of $C_{l,\max}$ and an increase in C_d. They increase the dependence of C_m on α, hasten the break in C_m, and induce thin-airfoil stall as characterized by McCullough and Gault [4].

Two common types of ice accretion simulations for use in wind tunnels are castings and 2-D smooth simulations. Castings capture nearly all of the three dimensionality and detail of the ice accretion and are generally considered a simulation that can produce the true aerodynamics of the accretion. The casting used in this study was created from a mold of an ice accretion generated in an icing wind

Presented as Paper 0087 at the 45th AIAA Aerospace Sciences Meeting & Exhibit, Reno, NV, 8–11 January 2007; received 24 May 2007; revision received 12 October 2007; accepted for publication 13 October 2007.

*Graduate Research Assistant, Department of Aerospace Engineering. Member AIAA.

†Research Scientist, Department of Aerospace Engineering. Senior Member AIAA.

‡Professor of Aerospace Engineering, Associate Dean for Research and Administrative Affairs. Fellow AIAA.

tunnel using the techniques described by Addy et al. [5]. A 2-D smooth simulation is made by tracing either the ice accretion or a casting of the ice accretion. This tracing, which is sometimes smoothed, is extruded to form a constant cross-section simulation with horn geometry representative of the accretion at the corresponding spanwise station.

Several studies have been conducted comparing the aerodynamic performance of a casting and a 2-D smooth simulation of the same ice accretion. Gurbacki and Bragg [6] compared a casting of a horn-ice accretion on a NACA 0012 to a 2-D smooth simulation of the same accretion. It was found that the casting had a higher $C_{l,\max}$ and a shorter separation bubble than the 2-D smooth simulation. However, other tests comparing a casting to a 2-D smooth simulation have had different results. Addy and Chung [7] investigated a horn-ice shape on an NLF-0414 airfoil and found that the 2-D smooth simulation had a higher $C_{l\max}$ than the casting. In another comparison between a casting and a 2-D smooth horn-ice simulation performed by Addy et al. [8] on an airfoil similar to the GLC-305, both simulations had the same penalty to $C_{l\max}$.

All of the 2-D smooth simulations in these studies were fabricated based on a tracing of the ice accretion. When spanwise variation is present on the accretion, the location of the tracing may become important. If the horn simulation has an unrepresentative angle, surface location, radius, or height, then it could yield a different aerodynamic penalty. The differences seen in the studies just mentioned could be a result of the tracing location. Because the 2-D model was extruded directly from smoothed versions of the tracing, the 2-D simulation of the casting has slightly different geometric parameters than the casting. It is important to note that the measured differences in critical performance parameters, such as $C_{l,\max}$, between 2-D and 3-D ice simulations is usually much less than the degradation from the clean case. Nonetheless, it is important for a comprehensive simulation study to understand why these differences exist.

The aerodynamic effects of parametrically varying the ice-horn geometry have been investigated in several studies, but these studies examined only large variations in horn height. Kim and Bragg [9] used an NLF-0414 airfoil to simulate three horn heights at various surface locations and with different tip radii. The smallest horn had a height $k/c = 0.0222$ with the taller horns being double and triple this height. Broeren et al. [10] performed a similar test on NACA 23012 and 3415 airfoils. Additionally, Papadakis et al. [11] simulated a horn with height $k/c = 0.0625$ at several surface locations on a NACA 0011. A horn double this size ($k/c = 0.125$) was then tested at the same locations. In all of these tests, horn height was found to be a significant factor in determining the penalty to $C_{l,\max}$. However, these studies were intended to evaluate the aerodynamic penalties of various ice shapes. They were not intended to determine the effect of small variations in horn height that could result from differences in quantifying the geometry of a particular ice shape from a tracing.

Several types of simulations other than castings and 2-D smooth simulations may also be used to model the aerodynamics of an ice accretion. Two-dimensional simple geometric simulations are of a lower fidelity than 2-D smooth simulations and are even easier to construct. These simulations are generated by using simple geometric shapes, such as triangles or rectangles, which imitate the main features of the ice accretion. As with 2-D smooth simulations, 2-D simple geometric simulations do not capture any of the spanwise variation present in the original ice accretion. However, they can be manufactured even more quickly and inexpensively. This makes them ideal for use in parametric studies, such as those of Kim and Bragg [9], Papadakis et al. [11], and Lee [12]. Other types of simulations include 2-D smooth or simple geometric simulations with either nonperiodic or periodic spanwise variation. These simulations represent in part the spanwise variation of the basic geometric features of the ice accretion, but do not model the highly three-dimensional features such as ice feathers or nodules. Additionally, surface roughness may be added to change the fidelity of any of these simulations.

The effect of surface roughness on a horn-ice simulation is unclear. In one fluorescent oil-flow visualization study [13], it was found that adding roughness to a 2-D smooth ice shape caused the separation bubble reattachment zone to move approximately 5–10% farther upstream and generated three-dimensional flow features similar to those seen on the casting. No performance data were taken in this study, so the effect of the roughness elements on $C_{l,\max}$ was not determined. Another study by Addy et al. [8] found that the addition of 30-grit roughness had no effect on the airfoil $C_{l,\max}$ and only a minor effect on C_d. The authors cautioned that different methods of applying roughness may yield varying results. For example, there are no standardized methods for determining the appropriate roughness size and concentration, and there are different interpretations of what type of roughness will provide the best representation of an ice accretion.

The objective of the current experimental study was to determine the level of geometric simulation detail required to aerodynamically represent a horn-ice accretion in a wind tunnel. Two castings were created from ice accreted on NACA 0012 and NACA 23012 airfoils in icing wind tunnels. The NACA 0012 casting was used to construct a 2-D smooth simulation with removable horns of varying geometry for testing on a NACA 0012 airfoil. This simulation was used to quantify the sensitivity of small changes in ice-horn geometry on airfoil performance so that the effect of making tracings at different spanwise stations could be determined. Using this information, the NACA 23012 casting was traced and a set of 2-D simulations and 3-D simple geometric simulations of varying fidelity was constructed for testing on a NACA 23012 airfoil. The aerodynamic performance of these NACA 23012 simulations was then compared to that of the NACA 23012 casting. All aerodynamic testing was performed in the University of Illinois 3×4 ft wind tunnel at $Re = 1.8 \times 10^6$ and $M = 0.18$ on 18-in. chord airfoil models.

Experimental Methods

The aerodynamic testing in this study was conducted in the University of Illinois subsonic, low-turbulence, open-return wind tunnel, which had a test section measuring 2.8 ft high, 4 ft wide, and 8 ft long. Two airfoil models were used: a NACA 0012 and a NACA 23012. Both models had a chord of 18 in., a span of 33.563 in., and a removable leading edge to facilitate simple installation of ice accretion simulations. With the ice simulations installed, the NACA 23012 had a primary row of 73 taps located at 51% span and the NACA 0012 had a primary row of 61 taps at a 15-deg angle relative to the model centerline (beginning at midspan). The wind-tunnel and airfoil models are described in more detail by Busch [14].

All testing was conducted at $Re = 1.8 \times 10^6$ and $M = 0.18$. Lift and pitching-moment coefficient data were calculated by integrating airfoil surface pressures measured by an electronically scanned pressure system. Using standard momentum-deficit methods, the drag coefficient was computed from total pressure measurements collected by a traversable wake rake, shown installed behind the airfoil model in Fig. 1. For some of the ice simulations, there was significant variation in C_d when measured at different spanwise stations, especially at low angles of attack. This variation introduced additional uncertainty when making C_d comparisons, and was accounted for by measuring C_d at several spanwise stations for selected simulations. Although these measurements were taken into consideration and are discussed in the results, they are not directly presented in this paper. All C_d values reported here were measured with the wake rake located at a single spanwise station of 3.63 in. above the primary row of pressure taps. All data reported here were corrected for wind-tunnel wall effects using the methods of Allen and Vincenti [15] and Rae and Pope [16]. Busch [14] and Blumenthal [17] describe the experimental setup in more detail. Experimental uncertainties were calculated using the methods of Kline and McClintock [18] and Coleman and Steele [19], and a summary of these uncertainties is given in Table 1. Although the relative uncertainty of C_m appears to be large because the reference value is small, the absolute uncertainty is reasonable.

Fluorescent oil-flow visualization studies were also performed on selected simulations. For these studies, the airfoil model was coated with fluorescent oil that responded to the surface shear stress.

Fig. 1 Traversable wake rake installed behind the NACA 23012 airfoil model.

Regions of high shear caused more oil movement than regions of low shear, so these regions do not appear to be as bright as the low shear stress regions. Using this technique, the flowfield was examined to identify time-averaged separation bubble reattachment zones as well as regions of separation and reverse flow. The center of the time-averaged separation bubble reattachment zone could be estimated to within $x/c = \pm 0.02$ using this method.

NACA 0012 Ice Simulations

Both a casting and 2-D smooth geometries were tested on a NACA 0012 airfoil. The casting was produced from a mold of an ice accretion on an 18-in. chord NACA 0012 model in a separate icing test [6], the conditions of which are given in Table 2. The casting was traced to generate a 2-D smooth simulation, but the selection of spanwise stations at which the tracing could be made was substantially limited because the original casting was only 12 in. long. Duplicates had to be constructed and placed next to each other to fill the span of the model, and the end-to-end alignment of these duplicates depended on the spanwise station at which the tracing was made. Therefore, the location which seemed to both represent the overall horn geometry and provide duplicate casting alignment was chosen. The casting was instrumented with a pressure slice, which has been shown to yield accurate pressure measurements [17].

The tracing of the casting (identical to that of the tall upper-horn simulation in Fig. 2) was smoothed using 50% control points in SmaggIce [20] and extruded to generate a 2-D smooth simulation. This simulation was designed so that the upper and lower horns could be detached individually and replaced by a horn of a different size or shape. Pressure taps were installed in each of the horns as well as the base simulation; the locations of these taps are shown in Fig. 2.

Four different upper-horn geometries were tested, referred to as the tall, medium, short, and sharp upper-horn geometries (Fig. 2). The tall upper horn represents the horn geometry that matched the pressure slice of the casting, and was made from a tracing taken at a high point on the casting. The short upper horn represents the horn geometry that would result from a tracing made at a low point on the casting. The medium upper horn was chosen to be approximately midway between the tall and short upper horns. The sharp upper horn has the same height as the tall upper horn but a smaller tip radius, reflecting locations on the casting where the horn was sharper than the spanwise station at which the tracing was made. Three lower-horn geometries were also tested while the upper-horn geometry was held constant (using the tall upper horn). These three lower-horn geometries were designed the same way as the upper-horn geometries.

NACA 23012 Ice Simulations

The NACA 23012 ice simulations were based on horn-ice accreted in the NASA Glenn Icing Research Tunnel. The conditions under which the ice was accreted are given in Table 3 and are derived from those that a full-scale commercial turboprop aircraft with an airfoil similar to a NACA 23012 might experience during cruise flight. Anderson showed constant Weber number scaling to be an effective method of scaling ice shapes [21], and a modified version of this method was used in the current study. The velocity was kept constant between the full-scale and the subscale cases, which has been shown to have little effect on the accretion geometry [22,23], and the median volumetric diameter of the water droplets was adjusted such that it was within the range that could be produced by the icing tunnel. Blumenthal [17] describes in more detail the testing that yielded the NACA 23012 horn-ice accretion investigated in this paper.

Several different simulations of varying fidelities were used to model the aerodynamics of this accretion. The highest-fidelity simulation was a casting (Fig. 3a), which captures the three dimensionality of the original ice accretion and is the most representative simulation. The other simulations investigated were manufactured using rapid prototyping techniques. One of these was a simple geometric simulation with nonperiodic spanwise variation of the upper- and lower-horn height and angle. This simulation was designed from measurements of the upper- and lower-horn height and angle on the casting. These parameters were measured every 0.1 in. along the 11.2-in. span of the casting. The nonperiodic simple geometric simulation used rectangles whose size and orientation varied every 0.1 in. along the span of the simulation to simulate a horn with a height and angle representative of the horn on the casting. This simulation is shown in Fig. 3b.

Other types of simulations tested were simple geometric simulations with uniform periodic variation of the horn height only. A statistical analysis was performed on the spanwise measurements discussed above to determine the average and rms horn height and angle. The average horn height was $k/c = 0.047$ for the upper horn and $k/c = 0.032$ for the lower horn. The rms horn height was $k/c = 0.0032$ and $k/c = 0.0028$ for the upper and lower horns, respectively. A 4096-point fast Fourier transform analysis was also performed on the spanwise measurements, and it was determined that the dominant period was 1.6 in. Two simulations with uniform periodic variations were then made, one with a period of 1.6 in. (Fig. 3c) and one with a period of 0.8 in. The amplitude of the height variations for both of these simulations was 1 standard deviation.

The remaining simulations had a constant cross section. One of these simulations, a 2-D smooth simulation, was generated by making a tracing of the casting at the spanwise station at which the taps were located and extruding it over the span of the model (Fig. 3d). This spanwise station was carefully selected to ensure that it was representative of the overall ice accretion geometry. The final

Table 1 Sample uncertainties based on clean NACA 23012 airfoil data at $\alpha = 4$ deg and $Re = 1.8 \times 10^6$

Parameter	Reference value	Absolute uncertainty	Relative uncertainty, %
α	4.13	± 0.02 deg	± 0.48
C_l	0.556	± 0.000862	± 0.16
C_d	0.0071	± 0.000136	± 1.91
C_m	-0.0015	± 0.000269	± 17.38
C_p	-0.962	± 0.00448	± 0.47

Table 2 Icing conditions for NACA 0012 horn-ice accretion

Icing conditions—run 281 horn ice on NACA 0012 airfoil	
Velocity, kt	175
α, deg	4.0
Median volumetric diameter, μm	20
Liquid water content, g/m^3	0.55
T_t, °F/°C	27.5/ − 2.5
Exposure time, min	3.5

Table 3 Icing conditions for NACA 23012 horn-ice accretion

Icing conditions—run EDO735 horn ice on NACA 23012 Airfoil	
Velocity, kt	200
α, deg	2.0
MVD, μm	15.4
LWC, g/m^3	0.75
T_t, °F/°C	28.0/ − 2.2
Exposure time, min	5.0

simulation was created by emulating the horn using simple geometric shapes (rectangles). The cross sections and pressure tap locations for these two simulations are shown in Fig. 4. Because the span of each of the simulations was only 11.2 in. and the airfoil model was 33.6 in., three identical simulations of each type were constructed and placed end to end to form a 33.6-in. long ice shape.

Finally, roughness elements of various sizes were added to each of the simulations (except the casting) to model the roughness of the ice accretion. Two different types of roughness elements were used: 14 grit silicon carbide and size 35/40 glass microbeads. Based on measurements of individual particles, these roughness elements had heights of $k/c = 0.0033$ and $k/c = 0.0009$, respectively. The $k/c = 0.0033$ roughness elements were irregularly shaped and jagged, whereas the $k/c = 0.0009$ roughness elements were spherical. The $k/c = 0.0033$ roughness was applied at a 50% concentration and the $k/c = 0.0009$ roughness was applied at an 80% concentration. The addition of these roughness elements added a small-scale three dimensionality to each of the simulations.

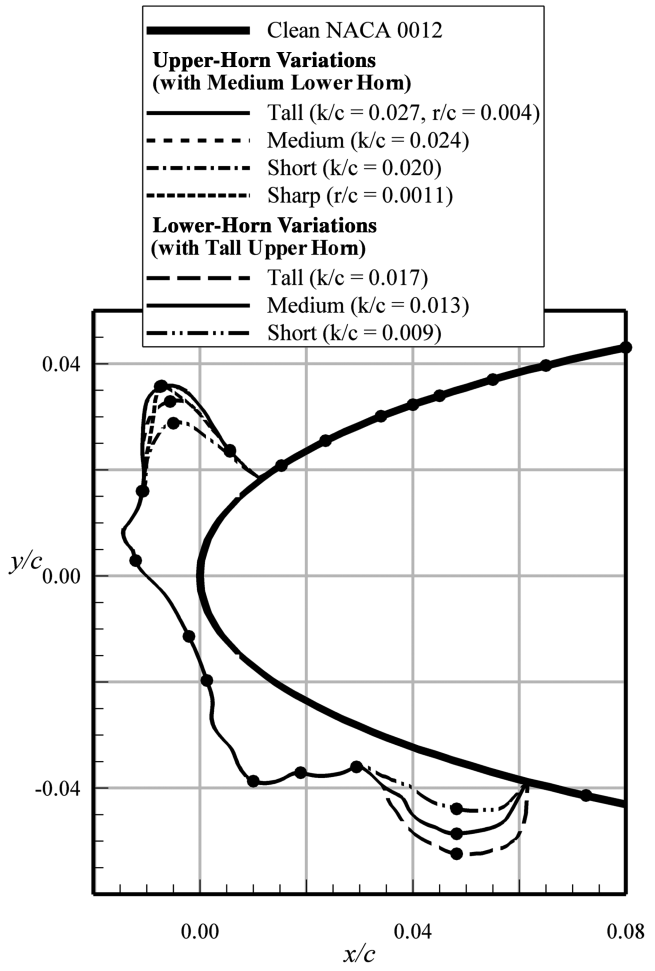

Fig. 2 Parametric variation of horn geometries tested on the NACA 0012 airfoil. The black circles indicate pressure tap locations.

Results and Discussion

Effects of Horn Geometry

The effects of the horn-ice simulations on the NACA 0012 airfoil performance are summarized in Fig. 5. The casting caused the NACA 0012 airfoil to exhibit thin-airfoil stall and decreased $C_{l,\max}$ by 58% to 0.56 (Fig. 5a). In this paper, the α at which $C_{l,\max}$ is achieved is reported as α_{stall}. This occurred at $\alpha = 7.1$ deg. The horn-ice casting also increased the dependence of C_m on α considerably and caused $C_{d,\min}$ to increase by 355% to 0.0297 (Fig. 5b).

The variations in the upper-horn height and radius considerably affected $C_{l,\max}$, C_m, and C_d. The 2-D smooth simulation with the tall upper horn (and the medium lower horn) had the $C_{l,\max}$ that was closest to that of the casting, differing by only 2%. The $C_{l,\max}$ increased by 6% (relative to the casting) for the medium upper horn and by 11% for the short upper horn. Also, airfoil stall was delayed by 1 deg for these two horns.

Decreasing the upper-surface horn tip radius also affected $C_{l,\max}$, decreasing it by 8% and causing stall to occur at least 1 deg earlier than the casting. This contrasts with an earlier parametric study using simple geometric shapes on an NLF-0414 in which changes in the upper-surface horn tip radius affected $C_{l,\max}$ by less than 2% [24]. On the NLF-0414, the horn had a height of $k/c = 0.022$ at a location of $s/c = 0.017$. The horn tip radius was varied from 1.10 to 0%, whereas the tip radius of this study's horn on the NACA 0012 was varied from 0.39 to 0.11%. A much smaller change in tip radius had a larger effect on the $C_{l,\max}$ of the NACA 0012. This suggests that some airfoil and ice-shape geometries may be more sensitive to horn tip radius than are others.

Changes in the height and tip radius of the upper horn also caused substantial changes in C_d (Fig. 5b). The tall upper-surface horn had a $C_{d,\min}$ 17% below that of the casting at $\alpha = 0.0$ deg. The higher C_d of the casting around $\alpha = 0$ deg was at least in part caused by surface roughness, as was confirmed by the addition of roughness elements to the tall upper-surface horn simulation (see Blumenthal et al. [25] for details). As α increased, the effect of the large separation bubble behind the horn became larger relative to the effect of the surface roughness, so C_d of the two simulations converged.

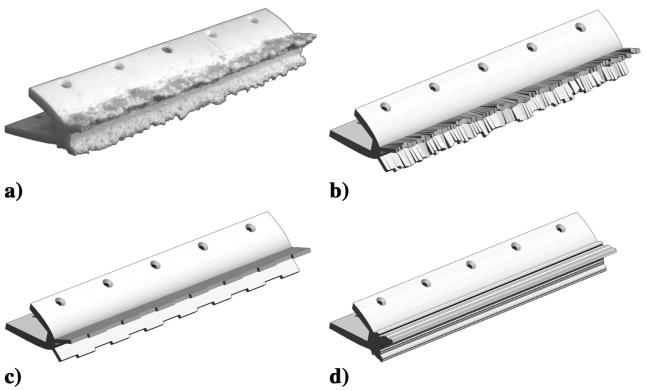

Fig. 3 Simulations of NACA 23012 horn-ice accretion: a) casting, b) simple geometric with nonperiodic spanwise variation, c) simple geometric with periodic spanwise variation, and d) 2-D smooth simulations. Each simulation can be mounted on a removable leading edge on the airfoil model.

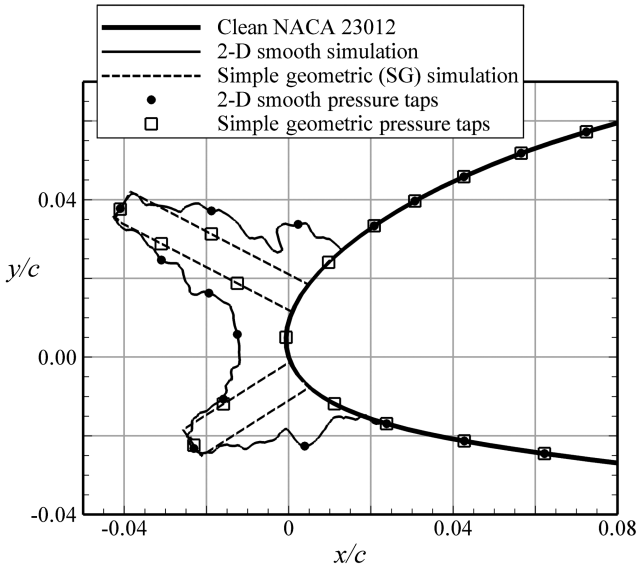

Fig. 4 Cross sections of the 2-D smooth and simple geometric simulations of the NACA 23012 horn-ice accretion.

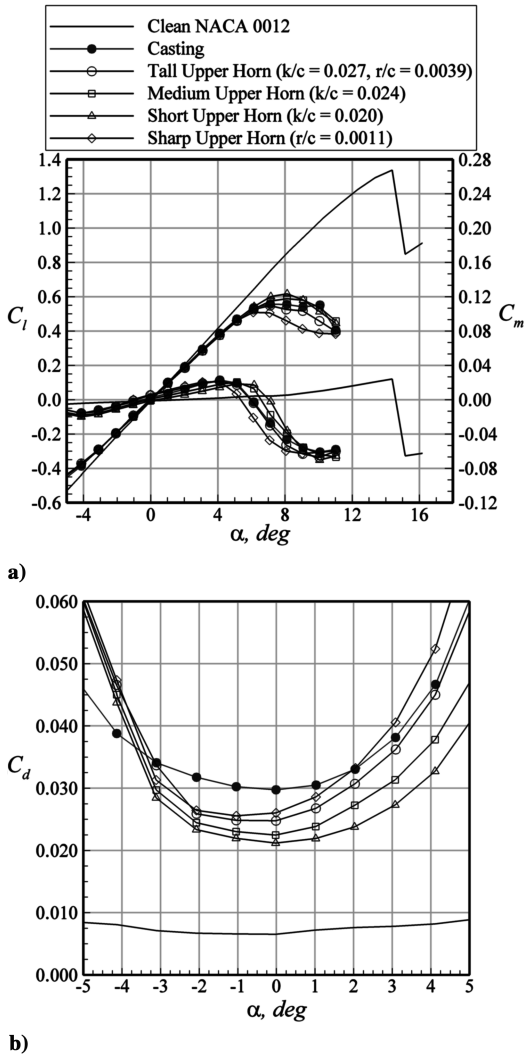

Fig. 5 Comparison of a) C_l, C_m, and b) C_d for the various upper-horn geometries on the NACA 0012.

For the medium and short upper-surface horn simulations, C_d tended to decrease with decreasing horn height at all angles of attack. The sharp upper horn had a $C_{d,\min} = 0.0260$ at $\alpha = 0.0$ deg, approximately 13% lower than C_d of the casting. As the angle of attack increased, the difference in drag between each of the 2-D simulations became more pronounced. This was likely caused by the larger differences in separation bubble length due to the different horn geometries at higher angles of attack.

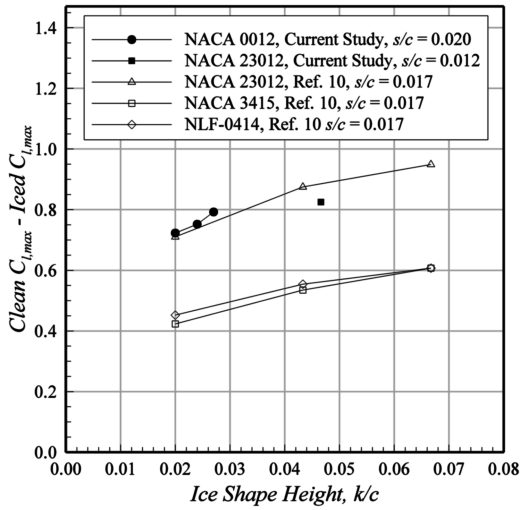

Fig. 6 Comparison of results between the current study and a previous study by Broeren et al. [10].

The results for the degradation in $C_{l,\max}$ agree with an earlier study by Broeren et al. [10] on NACA 23012, NACA 3415, and NLF-0414 airfoils, providing evidence that the above $C_{l,\max}$ trends of the current study are reasonable. In that study, the horn height, tip radius, and location were each varied parametrically using simple geometric simulations. Both the NACA 0012 and NACA 23012 data from the current study are superimposed on the data from the previous study in Fig. 6 (in the current study, the horn was located at $s/c = 0.020$ on the NACA 0012 and $s/c = 0.012$ on the NACA 23012; in the previous study, it was located at $s/c = 0.017$ for each airfoil). The NACA 23012 horn-ice simulation in this study caused a smaller aerodynamic penalty than the simulation of Broeren et al. [10] because the horn was located closer to the leading edge. Kim and Bragg [9] showed that $C_{l,\max}$ tends to decrease as s/c increases for a horn of a given height. With this consideration, the differences in $C_{l,\max}$ due to changes in horn height were consistent between the two studies for the NACA 0012 and NACA 23012; the penalty to these airfoils was likely similar because they both derive their lift mainly from a large suction peak near their leading edges. The NACA 3415 and NLF-0414 were less affected by the ice shape because they are more uniformly loaded [10].

The pressure distributions around the airfoil for each of the upper horns at $\alpha = 4.1$ deg are shown in Fig. 7. For each simulation, the pressure distribution shows a pressure plateau beginning behind the tip of the horn, indicative of a separation bubble. At $\alpha = 4.1$ deg, this plateau is followed by a steep pressure recovery resulting from the increase in flow momentum near the airfoil surface due to shear-layer transition. Because no flow visualization was conducted on the NACA 0012 ice simulations, the pressure distributions were used to qualitatively compare the separation bubble reattachment location of each simulation. The intersection of the clean and iced-airfoil pressure distributions downstream of the pressure plateau is the approximate reattachment location [26], although recent studies have shown reattachment may occur several percent chord beyond this intersection [14,17,27].

The differences in lift and pitching moment seen in Fig. 5 can be explained by the relative sizes of the separation bubble downstream of each of the horn simulations. Because the separation bubble grows with increasing angle of attack at approximately the same rate for each simulation and thin-airfoil stall occurs when the separation bubble reattachment zone moves off the airfoil trailing edge, simulations with larger separation bubbles will stall at a lower α than those with smaller separation bubbles. The short upper-horn simulation resulted in the smallest separation bubble and therefore the highest $C_{l,\max}$. The sharp upper-horn simulation had the largest

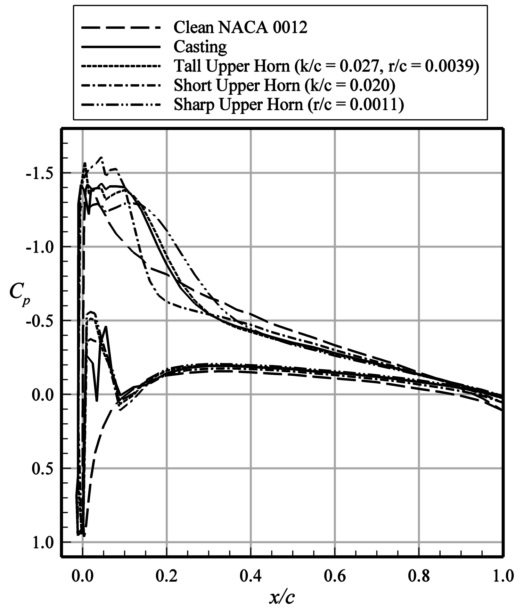

Fig. 7 Pressure distributions for various upper-horn geometries on the NACA 0012 at $\alpha = 4.1$ deg.

separation bubble and thus the lowest $C_{l,\max}$. The reattachment location for the 2-D smooth simulation with a tall upper horn was only slightly farther downstream than that of the casting, which explains why $C_{l,\max}$ of these two simulations was so close. The effect of the ice simulations on C_m at $\alpha = 4.1$ deg was to prolong the suction at the leading edge on the upper surface of the airfoil. This caused an increase in C_m relative to the clean case, with larger separation bubbles causing larger increases.

The effects on lift and pitching moment due to modifying the lower-horn height were small compared to those encountered when modifying the upper horn geometry. However, C_d was notably affected at low angles of attack, with changes being on the order of those incurred by variations in the upper horn geometry. More details regarding the aerodynamic penalties due to modifications of the lower horn geometry can be found in Busch [14] and Blumenthal et al. [25].

This study demonstrated that a decrease in horn height of 11% could increase $C_{l,\max}$ by 7% and a sharp tip radius instead of a more rounded radius could decrease $C_{l,\max}$ by 8%. These differences in horn geometry are on the order of those due to spanwise variation and the differences in $C_{l,\max}$ are on the order of those seen in previous studies between castings and their corresponding 2-D smooth simulations. It is likely that the inconsistencies in previous studies resulted from the use of 2-D simulations which did not accurately represent the mean effective horn geometry of the casting. These results suggest that tracings of an ice shape must be made carefully. The location of the tracing must be chosen at a cross section that is representative of the geometry of the entire ice accretion. If a tracing of the accretion is made at a particularly high or sharp section of the horn, the 2-D smooth simulation will likely have a lower $C_{l,\max}$ and higher C_d than the corresponding casting. Focus should be placed on selecting the most characteristic location for the upper-horn tracing as variations in lower-horn height had a much smaller effect on $C_{l,\max}$ than did variations in upper-horn height. If possible, several tracings should be averaged together to form a single tracing that is more representative of the ice accretion. These results were taken into consideration when constructing simulations for testing on the NACA 23012 airfoil; this testing is described below.

Effects of Simulation Fidelity

Recall that three categories of simulations were constructed for a NACA 23012 to investigate the effects of geometric simulation fidelity on airfoil aerodynamics: a casting, two 2-D simulations, and three 3-D simple geometric simulations (Fig. 3). One of the 2-D

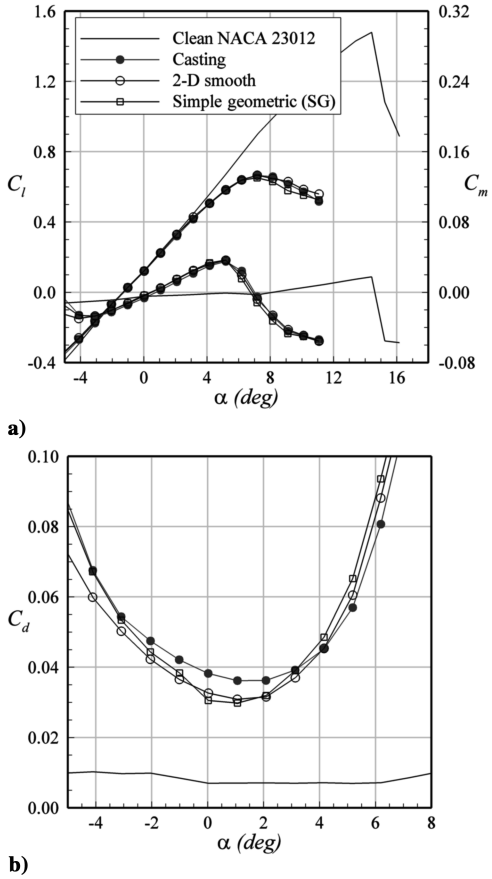

Fig. 8 Comparison of a) C_l, C_m, and b) C_d between the casting and each 2-D simulation on the NACA 23012.

simulations was a simple geometric simulation and the other was a 2-D smooth simulation. Two of the 3-D simple geometric simulations had periodic binary spanwise variation of the upper- and lower-horn height (with periods of 0.8 and 1.6 in.) and the third had nonperiodic spanwise variation of the height and angle of both horns at 0.1-in. increments.

The effects of the casting on C_l, C_m, and C_d of the NACA 23012 are shown in Fig. 8. The clean airfoil had a $C_{l,\max}$ of 1.48 at $\alpha = 14.4$ deg. and a $C_{d,\min}$ of 0.0070 at $\alpha = 0.0$ deg. The addition of the casting caused a 55% reduction in $C_{l,\max}$ and a 400% increase in $C_{d,\min}$. It also caused the airfoil to change from a leading-edge stall at $\alpha = 14.4$ deg. to a thin-airfoil stall at $\alpha = 7.2$ deg.

The 2-D smooth simulation had a $C_{l,\max}$ identical to that of the casting at the same stall angle of attack ($C_{l,\max} = 0.66$, $\alpha_{\text{stall}} = 7.2$ deg) and the simple geometric simulation had a 2% lower $C_{l,\max}$ of 0.65 (Fig. 8a). The stall type for each of the 2-D simulations was thin-airfoil stall and was very similar to that of the casting. The overall agreement in C_m was good, although both simulations had a slightly higher C_m than the casting at all positive angles of attack well below stall. At $\alpha = 5$ deg, the 2-D simulations had values of C_m within 5% of the casting. Beyond $\alpha = 5$ deg, the 2-D simulations both underestimated C_m.

A comparison of the C_d curves of the casting and the 2-D simulations is shown in Fig. 8b. At low angles of attack, C_d of both of the 2-D simulations was below that of the casting, although $C_{d,\min}$ occurred at $\alpha = 1.1$ deg for each of the simulations. As α increased, C_d of the 2-D simulations increased more rapidly than C_d of the casting, causing them to overestimate C_d at higher angles. The C_d values shown in Fig. 8b were obtained at a spanwise station located 3.63 in. above the pressure tap row. However, C_d was found to vary when measurements were taken across the span of the model. At $\alpha = 0.0$ deg (from 0.5 in. below the pressure tap row to 4.5 in. above the pressure tap row), C_d of the casting varied from 0.0303 to 0.0394, and C_d of the 2-D smooth simulation varied from 0.0305 to 0.0347. Thus, at this α, C_d of the 2-D smooth simulation fell within the range

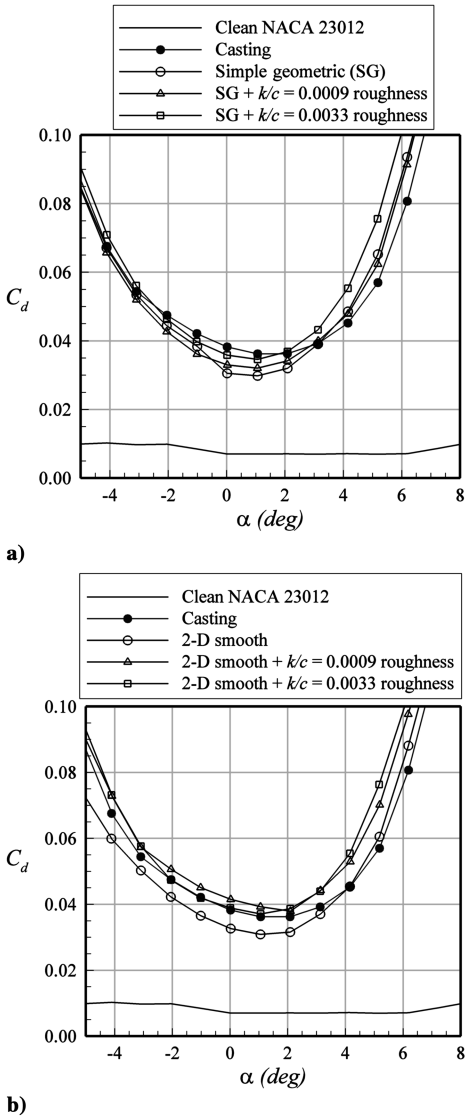

Fig. 9 Effect of surface roughness on C_d of the a) simple geometric and b) 2-D smooth horn-ice simulations on the NACA 23012.

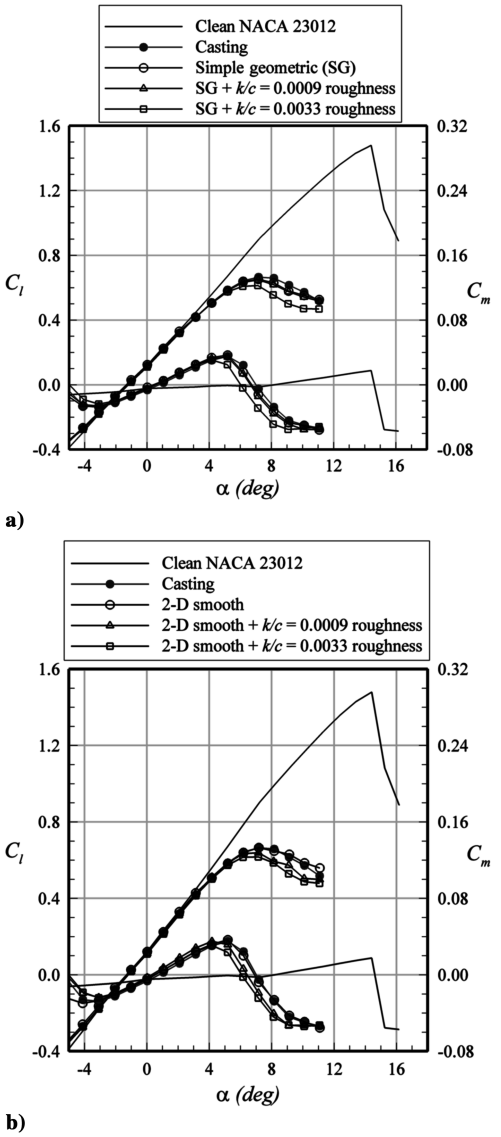

Fig. 10 Effect of surface roughness on C_l and C_m of the a) simple geometric and b) 2-D smooth horn-ice simulations on the NACA 23012.

of C_d of the casting due to spanwise variation (see Busch et al. [28] for more details). As α increased, the spanwise variation in C_d decreased. At $\alpha = 5$ deg, C_d of the casting varied from 0.0590 to 0.0623 and C_d of the 2-D smooth simulation varied from 0.0627 to 0.0644. The rms difference in C_d over several angles of attack is a useful metric for comparing the drag polar of a simulation to that of a casting. In this study, the rms difference in C_d was calculated over the linear α range, from -4 to 6 deg, because a goal of the study was to quantify the aerodynamic accuracy of a simulation over a wide range of α. The rms difference in C_d between the casting and the simple geometric simulation was 0.0062, and it was 0.0054 between the casting and the 2-D smooth simulation (from $\alpha = -4$ to 6 deg).

To determine if the higher C_d of the casting from $\alpha = -2$ to 2 deg may have been due to the rough surface of the casting, two different sizes of roughness ($k/c = 0.0009$ and $k/c = 0.0033$) were added to each of the 2-D simulations. The effects of this roughness on C_d are shown in Fig. 9. On the simple geometric simulation, the $k/c = 0.0009$ roughness made a noticeable difference in C_d only at angles of attack near $\alpha = 0$ deg, whereas the larger roughness size caused the entire C_d curve to shift upward. On the 2-D smooth simulation, both roughness sizes caused increases in C_d at all angles of attack. In general, added roughness shifted the C_d curve upward, increasing $C_{d,\min}$ and causing both the simple geometric and the 2-D smooth simulation C_d to more closely match the casting C_d at lower angles of attack. The roughness also caused a much larger C_d at higher angles of attack, suggesting that the added upper-surface roughness did not have the desired effect on the upper-surface flowfield and in most cases, the rms difference in C_d between the casting and the simulation from $\alpha = -4$ to 6 deg increased when roughness was added. The only exception was when $k/c = 0.0009$ roughness was added to the simple geometric simulation and the rms difference in C_d decreased to 0.0052, slightly better than for either simulation without roughness. However, the roughness present on the casting was much larger than the $k/c = 0.0009$ roughness, illustrating that it would be very difficult to determine the roughness size that would most accurately simulate the accretion aerodynamics without advance knowledge of these aerodynamics.

Roughness also had an effect on C_l, as shown in Fig. 10. The $k/c = 0.0009$ roughness affected $C_{l,\max}$ of the 2-D smooth simulation, decreasing it by 3%, but had no effect on the simple geometric simulation. The larger roughness size caused penalties to $C_{l,\max}$ of 8 and 7% for the simple geometric and 2-D smooth simulations, respectively. Both roughness sizes caused C_m to break approximately 1 deg earlier. Papadakis et al. [29] also investigated the effects of surface roughness on a horn-ice accretion. In that study, horn-ice shapes were generated by the NASA Glenn LEWICE 2.0 ice accretion code [30] for a swept wing using a GLC-305 airfoil, and the aerodynamic penalties both with and without the addition of $k/c = 0.0011$ roughness were measured. As in the present study, it was found that the addition of roughness tended to increase the aerodynamic penalties associated with the ice accretion simulations.

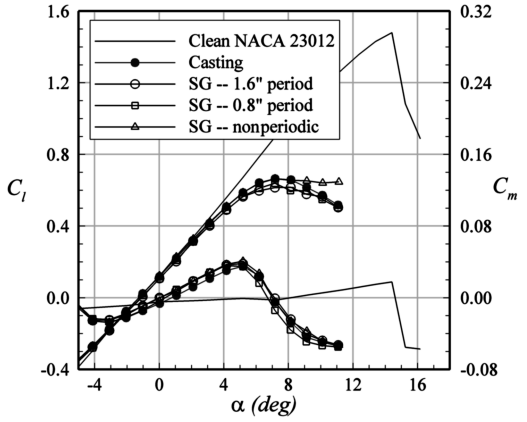

a)

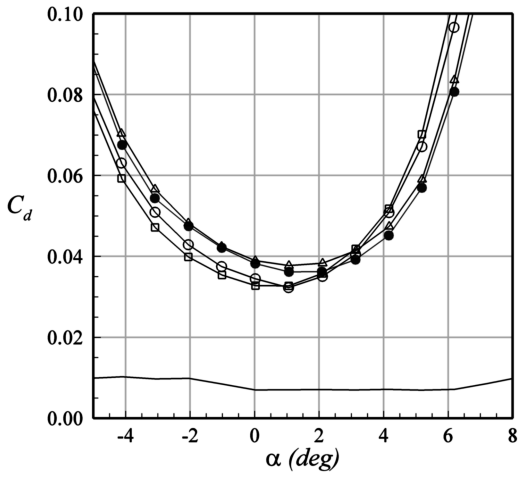

b)

Fig. 11 Comparison of a) C_l, C_m, and b) C_d between the casting and each 3-D simple geometric simulation on the NACA 23012.

In another study by Papadakis et al. [31], $k/c = 0.0012$ roughness was added to LEWICE shapes generated for a 24-in. chord 2-D airfoil model. Again, the addition of roughness was found to decrease $C_{l,\max}$ and increase C_d.

Because the $C_{l,\max}$ of these simulations agreed fairly well with the casting before roughness was added, roughness served only to decrease the agreement. Therefore, roughness, while noticeably affecting C_d, did not seem to significantly increase simulation accuracy in a predictable fashion when added in a uniform manner. One way to more accurately predict C_d might be to strategically size and position the roughness around the ice simulation to better tailor the drag performance versus angle of attack. For example, adding only lower surface roughness would likely increase C_d at low angles of attack, thereby improving the ability of the simulation to model C_d, but would have a minimal effect on $C_{l,\max}$. Unfortunately, this approach would be difficult without a priori knowledge of the true iced-airfoil aerodynamics.

The aerodynamic penalties due to each of the 3-D simple geometric simulations are compared with those of the casting in Fig. 11. The 0.8-in. period simulation underestimated $C_{l,\max}$ by 4%. The 1.6-in. period simulation had an even lower $C_{l,\max}$ (7% lower than the casting) but stalled 1 deg later than any of the other simulations. Because these two simulations had the same average horn height (which was also identical to that of the 2-D simple geometric simulation), it is evident that the period of the simulation had an effect on $C_{l,\max}$. The nonperiodic simulation had the same $C_{l,\max}$ as the casting. More so than for the 2-D simulations, every 3-D simulation overestimated C_m at positive angles of attack before stall.

The ability of each of the 3-D simple geometric simulations to model C_d of the casting is shown in Fig. 11b. The C_d curves of the two periodic simulations were very similar to each other, but are shifted by about 2 deg compared to the C_d curve of the casting. Each of these simulations also had a $C_{d,\min}$ approximately 10% lower than that of the casting. In general, the periodic simulations modeled C_d less accurately than did the 2-D simulations. The nonperiodic simulation, on the other hand, accurately simulated C_d at all angles of attack (Fig. 11b). The rms difference in C_d between the casting and the nonperiodic simulation was only 0.0021 from $\alpha = -4$ to 6 deg. This improvement may have been caused by the irregularities of the simulation due to the frequent change in cross-section geometry (in contrast to adding roughness or regular spanwise variation). This may provide a key to improving the modeling of C_d in the future.

Surface roughness was added to each of the 3-D simple geometric simulations in an attempt to improve their ability to estimate C_d. The 0.8 and 1.6-in. period simulations with added roughness were similar to each other in their ability to model the drag performance of the casting. The additional roughness had effects similar to those seen with the simple geometric shapes in Figs. 9a and 10a, in general causing a decrease in $C_{l,\max}$ and an increase in C_d. The same trends followed when roughness was added to the nonperiodic simple geometric simulation. Overall, roughness did not improve the modeling of either of these parameters. Additional details can be found in Busch [14].

The aerodynamic effects of each simulation are summarized in Table 4. The farthest left column shows the simulation type and the second column shows the difference in $C_{l,\max}$ between the simulation and the casting (with zero being perfect agreement). The third column shows the difference in α_{stall} between the simulation and the casting, and the last column shows the rms difference in C_d between the simulation and the casting over the range $\alpha = -4$ to 6 deg. Clearly, the nonperiodic simple geometric simulation most accurately modeled both $C_{l,\max}$ and C_d. Unfortunately, detailed measurements of the ice accretion horn height and angle must be made to fabricate this type of simulation, and accurately making these measurements poses additional challenges. A 2-D smooth simulation is much easier to construct and also had a $C_{l,\max}$ value similar to the casting. The addition of roughness to this type of simulation must be carefully considered, as it is difficult to gauge the appropriate roughness size to predictably improve simulation fidelity.

In addition to the performance data described above, flow visualization images were acquired for each type of ice simulation and are presented in Figs. 12–15 for $\alpha = 5$ deg. In the images, flow is from left to right, and the ice simulation is visible on the left. The horizontal scales at the top and bottom of the image correspond to the chordwise station in percent chord, while the vertical scale on the right measures the spanwise station in inches. The pressure tap row is located at the 0.0-in. spanwise station. As explained earlier, the severe adverse pressure gradient generated by the horn caused a

Table 4 Aerodynamic accuracy of various NACA 23012 horn-ice simulations

Simulation	Simulation $C_{l,\max}$ − casting $C_{l,\max}$	Simulation α_{stall} − casting α_{stall}, deg	RMS ΔC_d between simulation and casting $\alpha = -4$ to 6 deg
SG, nonperiodic	0.000	0.0	0.0021
2-D smooth	0.001	0.0	0.0054
SG	−0.013	0.0	0.0062
2-D smooth + $k/c = 0.0009$ roughness	−0.017	0.0	0.0079
SG + $k/c = 0.0009$ roughness	−0.020	0.0	0.0052
SG, 0.8-in. period	−0.026	0.0	0.0102
SG, 1.6-in. period	−0.051	0.9	0.0070

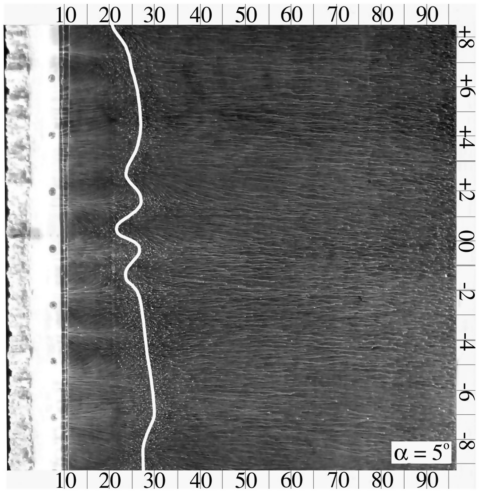

Fig. 12 Fluorescent oil-flow visualization of the casting on the NACA 23012 at $\alpha = 5$ deg. Flow is from left to right. The mean separation bubble reattachment line has been highlighted.

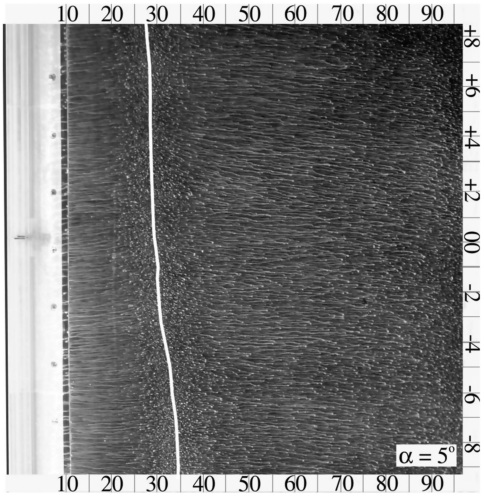

Fig. 13 Fluorescent oil-flow visualization image of the 2-D smooth horn-ice simulation on the NACA 23012 at $\alpha = 5$ deg. The mean separation bubble reattachment line has been highlighted.

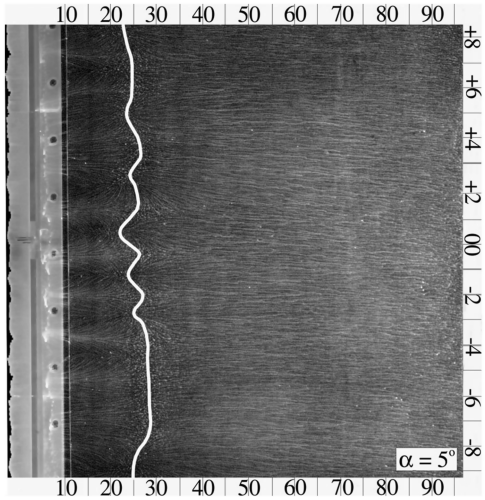

Fig. 14 Fluorescent oil-flow visualization image of the nonperiodic simulation on the NACA 23012 at $\alpha = 5$ deg. The mean separation bubble reattachment line has been highlighted.

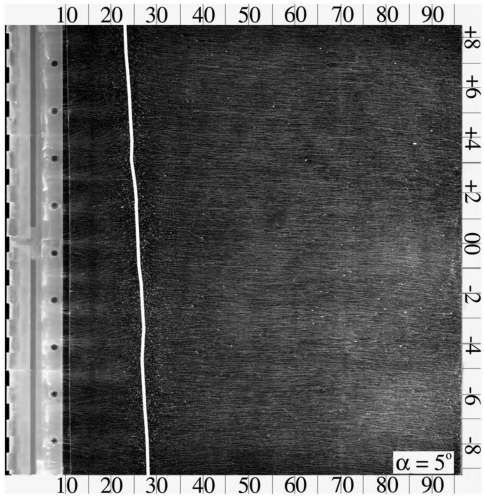

Fig. 15 Fluorescent oil-flow visualization image of the 1.6-in. period simulation on the NACA 23012 at $\alpha = 5$ deg. The mean separation bubble reattachment line has been highlighted.

separation bubble to form. The mean reattachment location of this separation bubble is evident in the flow visualization images and has been highlighted in each case. For the casting (Fig. 12), the reattachment location of the separation bubble ranges from $x/c = 0.21$ near the top and center of the model to $x/c = 0.30$ near the bottom of the model. Inside of the separation bubble is a region of reverse surface flow, indicated by the oil streaks flowing from right to left. The flowfield behind the casting is highly three dimensional, consisting of several spanwise cell structures similar to those seen in the studies of Gurbacki and Bragg [6] and Blumenthal [17]. Jacobs [32,33] performed extensive particle-image velocimetry (PIV) measurements of the flowfield behind both 2-D and 3-D horn-ice simulations on a NACA 0012 airfoil and characterized the structure of the streamwise vortices generated by the horn. In his study, the concentration of vortices was approximately uniform across the model span on the 2-D simulation. On the 3-D simulation, however, the vortex concentration was higher at certain locations along the span, resulting in increased shear stress at the airfoil surface and the cell structures seen in the flow visualization images.

The flow visualization image of the 2-D smooth simulation is shown in Fig. 13. The separation bubble reattachment zone ranged from approximately $x/c = 0.28$ to $x/c = 0.34$ at $\alpha = 5$ deg, and so was only slightly larger than the separation bubble of the casting. Unlike in the case of the casting, no three-dimensional cell structures were observed in the oil flow behind the horn. Flow visualization of the 2-D smooth simulation with $k/c = 0.0033$ roughness revealed a substantially longer separation bubble than was present for the 2-D smooth simulation without additional roughness, with the bubble not reattaching until approximately $x/c = 0.45$ to 0.52. This is consistent with the observed effects on C_l and C_d. Also, the flowfield had little spanwise variation. This contrasts with the study of Jacobs and Bragg [13], in which the addition of roughness caused cell structures to form similar to those seen in the flowfield of the casting.

Flow visualization images for the nonperiodic simulation (Fig. 14) reveal three-dimensional cell structures nearly identical to those seen with the casting. Both the size and spacing of the cells are similar and they are located at approximately the same spanwise stations. Reattachment occurred at nearly the same chordwise station and the mean reattachment line varied in the same manner for both the casting and the nonperiodic simulation. The 1.6-in. period simulation also demonstrated the cell structures (Fig. 15), but the cells did not accurately replicate those of the casting and did not cause spanwise variation in the separation bubble reattachment location. The spacing was dictated by the period of the simulation and the spanwise location of the cells corresponded to areas of low horn height. Neither of the periodic simulations nor the 2-D smooth simulations (with or without roughness) had as much spanwise variation in the reattachment zone location as did the casting and the nonperiodic simulation, suggesting that nonperiodic variation of the horn geometry is necessary to accurately model this feature of the flowfield behind the horn.

Conclusions

The results of the horn-geometry sensitivity study on the NACA 0012 ice simulations demonstrate the high sensitivity in iced-airfoil performance to small changes in horn geometry and the need to carefully choose an appropriate ice simulation. For cases when an ice tracing is used, care must be taken to select a spanwise location that is representative of the entire ice accretion. In particular, special attention should be paid to the upper horn because small variations will cause considerable changes in $C_{l,\max}$ and C_d. The lower horn is less critical, as small variations make a difference only in C_d and only at low angles of attack.

Using these results, 2-D smooth and simple geometric simulations were constructed from a representative tracing of a NACA 23012 horn-ice accretion. The 2-D smooth and the nonperiodic simple geometric simulations modeled $C_{l,\max}$ to within 1% of the casting $C_{l,\max}$ and the 2-D simple geometric simulation modeled $C_{l,\max}$ to within 2%. Significant spanwise variation was observed in the flowfield behind the casting. This variation was not present in the flowfield of either of the 2-D simulations, but was present in the flowfield of the 3-D simple geometric simulations. The nonperiodic simulation almost exactly reproduced the flowfield of the casting. This simulation most accurately modeled C_d over a wide range of angles of attack. At low angles of attack, C_d of the 2-D smooth simulation was within the range of the casting C_d due to spanwise variation. At high angles of attack, the 2-D smooth simulation C_d was only slightly higher than the casting C_d. Roughness may be able to improve the estimate of C_d, but, at this time, the appropriate roughness size cannot be easily determined without advance knowledge of the accretion aerodynamics. Construction of a simple geometric simulation with nonperiodic spanwise variation is challenging, as the accretion horn height and angle must be measured at many locations along the span. This process was simplified in this study because a casting of the accretion was available. It would be substantially more difficult to make these measurements on an actual ice accretion. The improvement in aerodynamic accuracy of the nonperiodic simulation may not be sufficient to outweigh the fabrication effort. Instead, a 2-D smooth simulation is recommended for most simulation needs. This type of simulation is relatively simple to construct and will model C_l, C_m, and C_d reasonably well provided that the upper horn geometry is accurately captured. Further research is recommended to better understand the variation in C_d along the model span so that future simulations may model C_d more accurately.

Acknowledgments

This work was made possible through NASA grants NCC3-1039 and NCC3-852 from the NASA John H. Glenn Research Center at Lewis Field. The authors thank Gene Addy from NASA Glenn and Sam Lee from ASRC Aerospace Corporation for their valuable support and assistance during the course of this investigation.

References

[1] Bragg, M., Broeren, A., Addy, H., Potapczuk, M., Guffond, D., and Montreuil, E., "Airfoil Ice-Accretion Aerodynamic Simulation," AIAA Paper 2007-0085, Jan. 2007.

[2] Bragg, M. B., Broeren, A. P., and Blumenthal, L. A., "Iced-Airfoil Aerodynamics," *Progress in Aerospace Sciences*, Vol. 41, No. 5, 2005, pp. 323–362. doi:10.1016/j.paerosci.2005.07.001

[3] Tani, I., "Low Speed Flows Involving Bubble Separations," *Progress in Aerospace Sciences*, Vol. 5, 1964, pp. 70–103. doi:10.1016/0376-0421(64)90004-1

[4] McCullough, G. B., and Gault, D. E., "Examples of Three Representative Types of Airfoil-Section Stall at Low Speed," NACA TN-2502, Sept. 1951.

[5] Addy, H. E., Potapczuk, M. G., and Sheldon, D. W., "Modern Airfoil Ice Accretions," NASA TM-107423, March 1997.

[6] Gurbacki, H. M., and Bragg, M. B., "Unsteady Aerodynamic Measurements on an Iced Airfoil," AIAA Paper 2002-0241, Jan. 2002.

[7] Addy, H. E., Jr., and Chung, J. J., "A Wind Tunnel Study of Icing Effects on a Natural Laminar Flow Airfoil," AIAA Paper 2000-0095, Jan. 2000.

[8] Addy, H. E., Jr., Broeren, A. P., Zoeckler, J. G., and Lee, S., "A Wind Tunnel Study of Icing Effects on a Business Jet Airfoil," AIAA Paper 2003-0727, Jan. 2003.

[9] Kim, H. S., and Bragg, M. B., "Effects of Leading-edge Ice Accretion Geometry on Airfoil Aerodynamics," AIAA Paper 99-3150, June 1999.

[10] Broeren, A. P., Lee, S., LaMarre, C. M., and Bragg, M. B., "Effect of Airfoil Geometry on Performance with Simulated Ice Accretions Volume 1: Experimental Investigation," Rept. DOT/FAA/AR-03/64, Aug. 2003.

[11] Papadakis, M., Alansatan, S., and Seltmann, M., "Experimental Study of Simulated Ice Shapes on a NACA 0011 Airfoil," AIAA Paper 1999-0096, Jan. 1999.

[12] Lee, S., "Effects of Supercooled Large Droplet Icing on Airfoil Aerodynamics," Ph.D. Dissertation, Department of Aeronautical and Astronautical Engineering, University of Illinois at Urbana–Champaign, Urbana, IL, 2001.

[13] Jacobs, J. J., and Bragg, M. B., "Particle Image Velocimetry Measurements of the Separation Bubble on an Iced Airfoil," AIAA Paper 2006-3646, June 2006.

[14] Busch, G. T., "Ice Accretion Aerodynamic Simulation on a Subscale Model," M.S. Thesis, Department of Aerospace Engineering, University of Illinois at Urbana–Champaign, Urbana, IL, 2006.

[15] Allen, H. J., and Vincenti, W. G., "Wall Interference in a Two-Dimensional-Flow Wind Tunnel, with Consideration of the Effect of Compressibility," NACA, Rept. 782, 1944.

[16] Rae, W. H., and Pope, A., *Low-Speed Wind Tunnel Testing*, Wiley, New York, 1984.

[17] Blumenthal, L. A., "Surface Pressure Measurement on a Three-Dimensional Ice Shape," M.S. Thesis, Department of Aerospace Engineering, University of Illinois, Urbana, IL, 2005.

[18] Kline, S., and McClintock, F. A., "Describing Uncertainties in SingleSample Experiments," *Mechanical Engineering*, Vol. 75, No. 1, 1953, pp. 3–8.

[19] Coleman, H. W., and Steele, W. G., *Experimentation and Uncertainty Analysis for Engineers*, Wiley-Interscience, New York, 1989.

[20] Vickerman, M. B., Choo, Y. K., Schilling, H. W., Baez, M., Braun, D. C., and Cotton, B. J., "Toward an Efficient Icing CFD Process Using an Interactive Software Toolkit—SmaggIce 2-D," AIAA Paper 2002-0380, Jan. 2002.

[21] Anderson, D. N., "Evaluation of Constant-Weber-Number Scaling for Icing Tests," AIAA Paper 1996-0636, Jan. 1996.

[22] Anderson, D. N., and Ruff, G. A., "Evaluation of Methods to Select Scale Velocities in Icing Scaling Tests," AIAA Paper 1999-0244, Jan. 1999.

[23] Anderson, D. N., "Effect of Velocity in Icing Scaling Tests," AIAA Paper 2000-0236, Jan. 2000.

[24] Kim, H., "Effects of Leading-Edge Ice Accretion Geometry on Airfoil Performance," M.S. Thesis, Department of Aerospace Engineering, University of Illinois, Urbana, IL, 2004.

[25] Blumenthal, L. A., Busch, G. T., Broeren, A. P., and Bragg, M. B., "Issues in Ice Accretion Simulation on a Subscale Model," AIAA Paper 2006-0262, Jan. 2006.

[26] Roberts, W., "Calculation of Laminar Separation Bubbles and Their Effect on Airfoil Performance," *AIAA Journal*, Vol. 18, No. 1, 1980, pp. 25–31.

[27] Gurbacki, H. M., "Ice-Induced Unsteady Flowfield Effects on Airfoil Performance," Ph.D. Dissertation, Department of Aeronautical and Astronautical Engineering, University of Illinois, Urbana, IL, 2003.

[28] Busch, G., Broeren, A., and Bragg, M., "Aerodynamic Simulation of a Horn-Ice Accretion on a Subscale Model," AIAA Paper 2007-0087, Jan. 2007.

[29] Papadakis, M., Yeong, H., Wong, S., Vargas, M., and Potapczuk, M., "Aerodynamic Performance of a Swept Wing with Ice Accretions," AIAA Paper 2003-0731, Jan. 2003.

[30] Wright, W. B., "User Manual for the NASA Glenn Ice Accretion Code LEWICE Version 2.0," NASA CR-1999-209409, Sept. 1999.

[31] Papadakis, M., Gile Laflin, B. E., Youssef, G. M., and Ratvasky, T. P., "Aerodynamic Scaling Experiments with Simulated Ice Accretions," AIAA Paper 2001-0833, Jan. 2001.

[32] Jacobs, J., "Iced Airfoil Separation Bubble Measurements by Particle Image Velocimetry," Ph.D. Dissertation, Department of Aerospace Engineering, University of Illinois, Urbana, IL, 2007.

[33] Jacobs, J., and Bragg, M., "Two- and Three-Dimensional Iced Airfoil Separation Bubble Measurements by Particle Image Velocimetry," AIAA Paper 2007-0088, Jan. 2007.